



OPEN ACCESS

EDITED BY

Sajjad Gharaghani,
University of Tehran, Iran

REVIEWED BY

Dharmendra Kumar Yadav,
Gachon University, Republic of Korea
Abhijit Dasgupta,
University of Kalyani, India

*CORRESPONDENCE

Eun Sook Hwang,
✉ eshwang@ewha.ac.kr
Yunjeong Park,
✉ yunjpark21@ewha.ac.kr

[†]These authors have contributed equally to this work

RECEIVED 27 November 2025

REVISED 19 February 2026

ACCEPTED 25 February 2026

PUBLISHED 12 March 2026

CITATION

Lee S, Yoon SJ, Lim J, Oh JH, Ryu J-S, Kim G, Kang H, Jo N, Lee S, Jang S, Lee Y, Park Y and Hwang ES (2026) PoMA-10: a dual-action antiviral disrupting SARS-CoV-2 Spike-ACE2 interaction and protecting lung tissue. *Front. Pharmacol.* 17:1755268. doi: 10.3389/fphar.2026.1755268

COPYRIGHT

© 2026 Lee, Yoon, Lim, Oh, Ryu, Kim, Kang, Jo, Lee, Jang, Lee, Park and Hwang. This is an open-access article distributed under the terms of the [Creative Commons Attribution License \(CC BY\)](https://creativecommons.org/licenses/by/4.0/). The use, distribution or reproduction in other forums is permitted, provided the original author(s) and the copyright owner(s) are credited and that the original publication in this journal is cited, in accordance with accepted academic practice. No use, distribution or reproduction is permitted which does not comply with these terms.

PoMA-10: a dual-action antiviral disrupting SARS-CoV-2 Spike-ACE2 interaction and protecting lung tissue

Soheun Lee^{1†}, Suh Jin Yoon^{1,2†}, Jihae Lim¹, Ji Hyun Oh¹, Jae-Sang Ryu¹, Gahee Kim³, Hyunwoo Kang⁴, Nayoon Jo^{1,2}, Sehan Lee⁴, Sunbok Jang^{1,2}, Yoonji Lee³, Yunjeong Park^{1*} and Eun Sook Hwang^{1,2*}

¹College of Pharmacy and Graduate School of Pharmaceutical Sciences, Ewha Womans University, Seoul, Republic of Korea, ²Graduate Program in Innovative Biomaterials Convergence, Ewha Womans University, Seoul, Republic of Korea, ³College of Pharmacy, Chung-Ang University, Seoul, Republic of Korea, ⁴HITS Inc., Seoul, Republic of Korea

This study aimed to identify small molecules that inhibit the binding of the SARS-CoV-2 Spike protein to its host receptor, angiotensin-converting enzyme 2 (ACE2), without impairing the enzymatic activity of ACE2. Such inhibitors may support the development of broad-spectrum antivirals and therapeutic strategies for emerging SARS-CoV-2 variants. Through extensive screening using both cell-free and cell-based assays, we identified phenoxy-methylaniline (PoMA) compounds as effective inhibitors of the SARS-CoV-2 Spike-ACE2 interaction. Among these, PoMA-10, featuring trifluoromethoxy and dimethylaniline moieties, exhibited the most potent inhibitory activity while preserving ACE2 enzymatic function. Computational modeling predicted direct binding of PoMA-10 to ACE2, which was corroborated by protein mobility shift assays. This was further substantiated by surface plasmon resonance analysis and molecular dynamics simulations, which confirmed the stable binding of PoMA-10 at an interface-adjacent site on ACE2 and the disruption of SARS-CoV-2 Spike-ACE2 interaction. In Vero cells, PoMA-10 significantly reduced infection by ancestral SARS-CoV-2 and the Delta and Gamma variants. Moreover, PoMA-10 alleviated lung epithelial cell damage and protected against lipopolysaccharide-induced lung injury *in vivo*. These findings demonstrate that PoMA-10 functions as a dual-action inhibitor blocking viral entry and protecting against lung injury, and highlight its potential as a therapeutic candidate in the management of COVID-19 and related pulmonary complications.

KEYWORDS

ACE2 inhibition, acute lung injury, phenoxy-methylaniline, SARS-CoV-2, spike protein

1 Introduction

Severe acute respiratory syndrome coronavirus 2 (SARS-CoV-2) has caused the COVID-19 pandemic, posing a major global health threat (Andersen et al., 2020; Billah et al., 2020; Narayanan et al., 2024). The high mutation rate of the virus, attributable to its low replication fidelity, has accelerated the convergence of variants (Peck and Lauring, 2018; Chen et al., 2022), thus creating a persistent threat to global health. Variants of concern, including Alpha, Beta, Gamma, Delta, and Omicron, display increased transmissibility and immune evasion, largely due to mutations in the receptor-binding domain (RBD) and N-terminal region of the Spike protein, which increase the

binding affinity of Spike protein to the host cell receptor, angiotensin-converting enzyme 2 (ACE2) (Scovino et al., 2022).

Several inhibitors have been developed to primarily target viral or host enzymes. These include the antiviral drug remdesivir (RDS); the ACE2 inhibitor captopril (CAP); the protease inhibitors camostat mesylate (CM) and nafamostat mesylate (NM); and the antimalarial drug chloroquine (CQ) (Jackson et al., 2022; Wang et al., 2022; Cui et al., 2024; Dong et al., 2024). Despite the significance of viral targets, the inhibitor of virus-receptor interactions remains an attractive antiviral strategy (Hoffmann et al., 2020a; Chitsike and Duerksen-Hughes, 2021; Meganck and Baric, 2021; Shapira et al., 2022). Small molecule therapeutics, in particular, offer advantages in terms of cell permeability, metabolic stability, and cost-effectiveness (Meganck and Baric, 2021; Kronenberger et al., 2023; Yang and Wang, 2023). Yet, the continuous emergence of variants and drug resistance underscores the urgent need for broadly effective SARS-CoV-2 entry blockers (Hu et al., 2023; Iketani et al., 2023; Jochmans et al., 2023; Kiso et al., 2023; Moghadasi et al., 2023).

Diphenyl ether moieties, found in marine-derived natural products, exhibit diverse biological activities, including antiviral against viruses like influenza and herpes, as well as herbicidal properties by interfering with plant growth and metabolism (Camilleri et al., 1988; Bunyapiboonsri et al., 2007). Inspired by the diphenyl ether scaffolds, we synthesized phenoxy-methylaniline (PoMA) derivatives—specifically CP1, CP2, and CP3—as core structures for further exploration as SARS-CoV-2 entry inhibitors. Additionally, to enhance their pharmacokinetic properties and binding affinity, we incorporated fluorine atoms, particularly focusing on trifluoromethoxy groups, which are well known recognized in medicinal chemistry for improving lipophilicity, metabolic stability, and membrane permeability (Haranahalli et al., 2019; Liu et al., 2022; Nair et al., 2022). These modifications aim to optimize the pharmacological profile of PoMA derivatives. Furthermore, we designed related compounds, CP4 and CP5, as antimicrobial peptide analogs to interfere with protein-protein interactions between SARS-CoV-2 Spike (hereafter referred to as Spike) protein and ACE2 (Park et al., 2015; Lee et al., 2024). In this study, we evaluated the effects of these PoMA derivatives, especially the fluorinated analogs, on Spike-ACE2 interactions and their potential to mitigate infection-driven inflammatory responses.

2 Materials and methods

2.1 Materials

CQ, CAP, CM, NM, RDS, MLN-4760, lipopolysaccharides (LPS), and Flag antibody were purchased from Sigma-Aldrich

(St. Louis, MO, United States). Compounds in the CP series and PoMA derivatives were synthesized and purified to 98% purity by High-performance liquid chromatography (HPLC) (Lee et al., 2024). Streptavidin-allophycocyanin (APC) (405207) was purchased from BioLegend (San Diego, CA, United States). Biotinylated SARS-CoV-2 (2019-nCoV) Spike RBD-His recombinant protein (40592-V08B-B) was purchased from Sino Biological (Wayne, PA, United States).

2.2 ACE2: Spike inhibitor screening assays

Screening and profiling of inhibitors of the Spike-ACE2 interaction were conducted using an ACE2: Spike RBD (SARS-CoV-2) inhibitor screening assay kit (BPS Bioscience Inc., #79936, San Diego, CA, United States) according to the manufacturer's instructions (Hoffmann et al., 2020a). In brief, a 96-well plate was coated with ACE2-His and subsequently incubated with Spike protein in the presence or absence of inhibitor compounds. The plate was washed and incubated with HRP-conjugated anti-His antibody, followed by chemiluminescence and immediate luminescence detection (Molecular Devices, Sunnyvale, CA, United States). The Spike-ACE2 blockers were additionally validated using two different inhibitor assay systems: the ACE2:Spike RBD and Spike:ACE2 binding colorimetric assay kits (RayBiotech Inc., CoV-ACE2S2 & CoV-SACE2, Peachtree Corners, GA, United States) using plate-bound ACE2 or Spike protein. Optical density was measured using a multifunctional microplate reader (Infinite 200 Pro microplate reader, Tecan, Switzerland) equipped at the Ewha Drug Development Research Core Center.

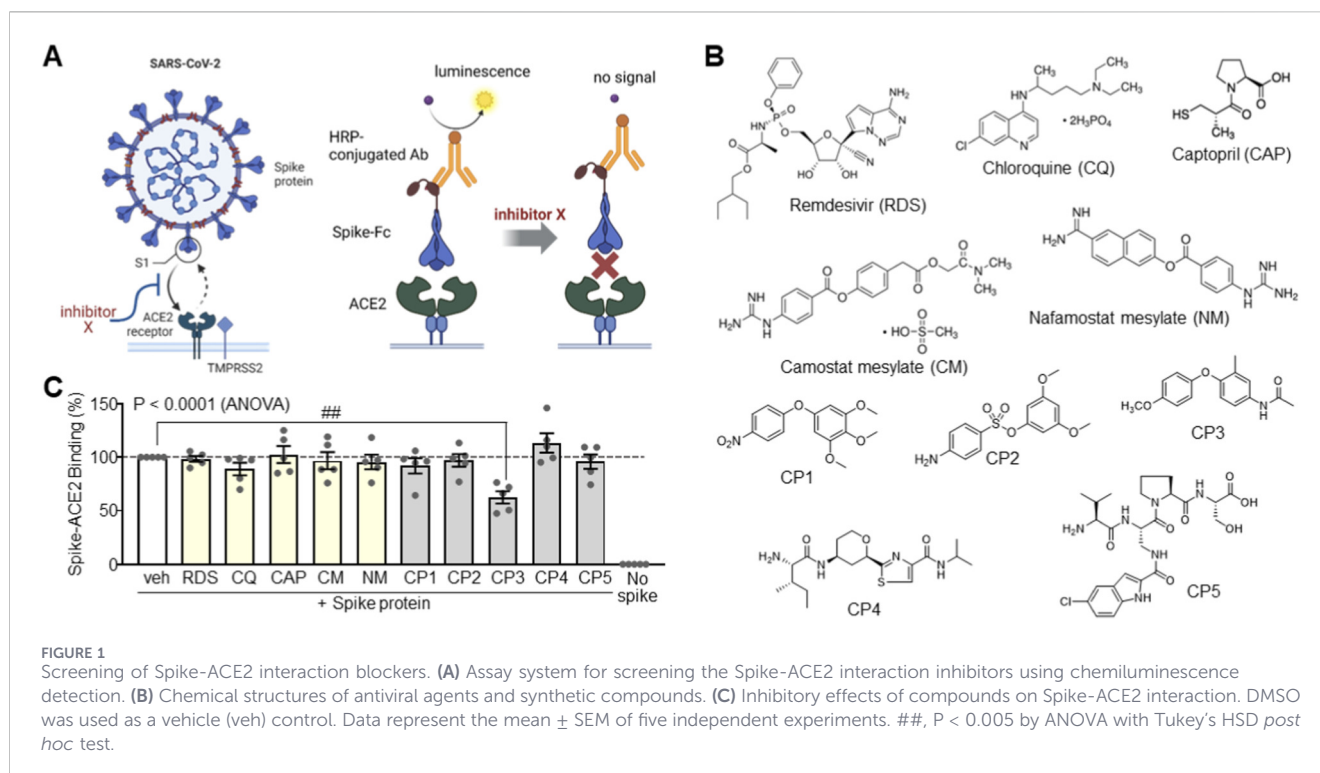
2.3 Cell-based Spike-hACE2 binding inhibition assay

BEAS-2B (ATCC, CRL-3588) and HEK293T (ATCC, CRL-3216) cells were maintained in DMEM with 10% FBS and transfected with pCMV3-human ACE2 (hACE2)-Flag plasmid DNA, followed by selection in the presence of hygromycin B (H772, Sigma-Aldrich). hACE2-BEAS-2B cells and hACE2-HEK293T cells expressing human ACE2 were established and subjected to the Spike binding assay. Cells (0.5×10^6 cells/mL) were incubated with 100 ng of biotinylated Spike protein in the presence of dimethyl sulfoxide (1% DMSO) control, PoMA-02 (100 μ M), PoMA-06 (100 μ M), or PoMA-10 (100 μ M) at 37 °C for 1 h. Dimethyl sulfoxide (1% DMSO) was added to the control. Cells were subsequently incubated with streptavidin-APC on ice for 20 min and analyzed using a FACS Calibur flow cytometer (BD Biosciences, San Jose, CA, United States). Cells were quantitated using the CellQuest software.

2.4 Molecular modeling

The X-ray crystal structure of ACE2 bound to the Spike protein (PDB ID: 6LZG) was prepared for docking by removing the Spike RBD chain and truncating all N-linked glycans (Wang et al., 2020); crystallographic water molecules were also removed. Ligands were generated and ionization states assigned at physiological pH, and induced-fit docking (IFD) was performed targeting the previously reported AlloSite3 pocket (Dutta, 2022). During IFD, residues

Abbreviations: ACE2, angiotensin-converting enzyme 2; ANOVA, analysis of variance; APC, allophycocyanin; BEAS-2B, human bronchial epithelial cell line; CAP, captopril; CM, camostat mesylate; COVID-19, coronavirus disease-19; CP, compound; CQ, chloroquine; HEK293T, human embryonic kidney 293-T cell line; IFD, induced-fit docking; LPS, lipopolysaccharides; MD, molecular dynamics; MM-GBSA, Molecular Mechanics, General Born Surface Area; NM, nafamostat mesylate; PoMA, phenoxy-methylaniline; RBD, receptor binding domain; RDS, remdesivir; RMSD, root-mean-square deviation; SARS-CoV-2, severe acute respiratory syndrome coronavirus 2; SEM, standard error of the mean.



within 5.0 Å of docked ligands were allowed to refine and side-chain optimization was carried out; 20 poses per ligand were re-docked and ranked. Predicted affinities were compared by MM-GBSA rescoring of minimized docked poses. Docking results were cross-validated against an independent ACE2 structure (PDB ID: 6M0J). Detailed procedures are provided in the Supplementary Information.

2.5 Molecular dynamics (MD) simulations

MD simulations started from the ACE2-Spike complex (PDB 6LZG) with the Spike placed ~ 5 Å from ACE2; resolved PTMs were parameterized with AmberTools. PoMA-10 RESP charges were computed at B3LYP/6-31G** (Psi4) and GAFF2 parameters were generated via ACPYPE. Simulations were carried out using GROMACS 2024.5 with AMBER ff14SB. Systems were energy-minimized, equilibrated through six restrained stages with restraints tapered to zero, then run in production. LINCS constrained bonds to hydrogen; PME handled electrostatics; van der Waals used 0.8–1.0 nm cutoffs with dispersion corrections. Temperature was 310 K (*v-rescale*) and pressure 1 bar (Parrinello-Rahman). Production timestep was 2 fs; coordinates every 10 ps and energies every 2 ps. Simulations continued without regenerating velocities; COM motion removed every 100 steps. Further technical details are provided in the Supplementary Information.

2.6 Protein mobility shift assay

hACE2-HEK293T cells expressing Flag-tagged hACE2 were harvested and extracted with extraction buffer (50 mM HEPES, pH 7.9, 150 mM NaCl, 0.1% NP-40, 10% glycerol) supplemented

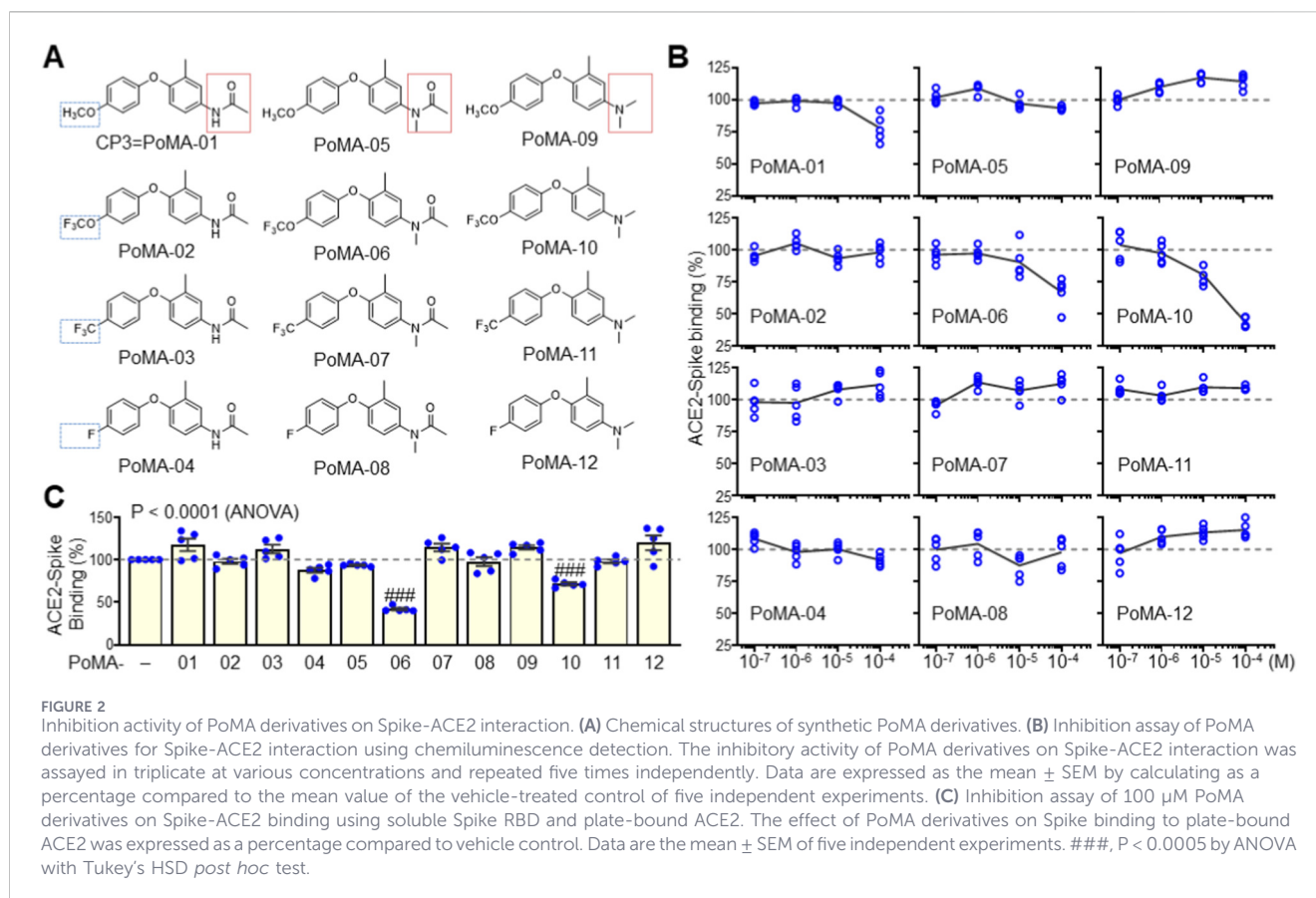
with protease and phosphatase inhibitors. Protein extracts containing hACE2 were reacted with PoMA-02, PoMA-06, or PoMA-10 for 15 min at room temperature and subjected to electrophoresis on a continuous 6% native acrylamide gel for 3 h, followed by immunoblotting analysis with anti-Flag antibody. NativeMark™ unstained protein standard (Thermo Fisher Scientific, LC0725) was used for size comparison in native gel electrophoresis. The migration distance of the hACE2 complex from the wells of the acrylamide gel was measured and calculated as a percentage of the vehicle control.

2.7 Surface plasmon resonance (SPR) assay

SPR experiments were performed using a Nicoya OpenSPR XT rev4 (carboxyl chip) (support from NFEC-2024-09-299613). After filtering and degassing buffers, chips were activated (EDC/NHS 1:1, 100 mM each, 600 s at 20 μ L/min) and ACE2 or Spike immobilized (50 μ g/mL in 10 mM sodium acetate, pH 5.0) at 4 °C (~ 1500 RU). Unreacted esters were blocked with 1 M ethanolamine-HCl (pH 8.5). Running buffer was PBS with 0.01% Tween-20, 0.5 mg/mL BSA, and 2% DMSO. PoMA-10 and PoMA-06 (50–200 μ M) were injected at 20 μ L/min; ACE2-PoMA-10 used 300 s association/dissociation, others used 300 s association and 600 s dissociation. Surfaces were regenerated with 10 mM glycine-HCl (pH 3.0, 40 s). Measurements were repeated and analyzed after reference subtraction; full details are in the Supplementary Information.

2.8 ACE2 enzyme activity assay

ACE2 enzyme activity was measured using a synthetic methoxycoumaryl acetyl (MCA)-based peptide substrate to



release a free fluorophore. An ACE2 Inhibitor Screening Kit (ab273373, Abcam, Cambridge, United Kingdom) was used for the ACE2 enzyme activity assay. In brief, a 96-well plate was incubated with diluted ACE2 enzyme, synthetic MCA-based peptide substrate, and different concentrations of inhibitor compounds. The plate was monitored in kinetic mode for 1 h using a fluorescence microplate reader (Molecular Devices) at the Ewha Fluorescence Core Imaging Center.

2.9 SARS-CoV-2 infection assay

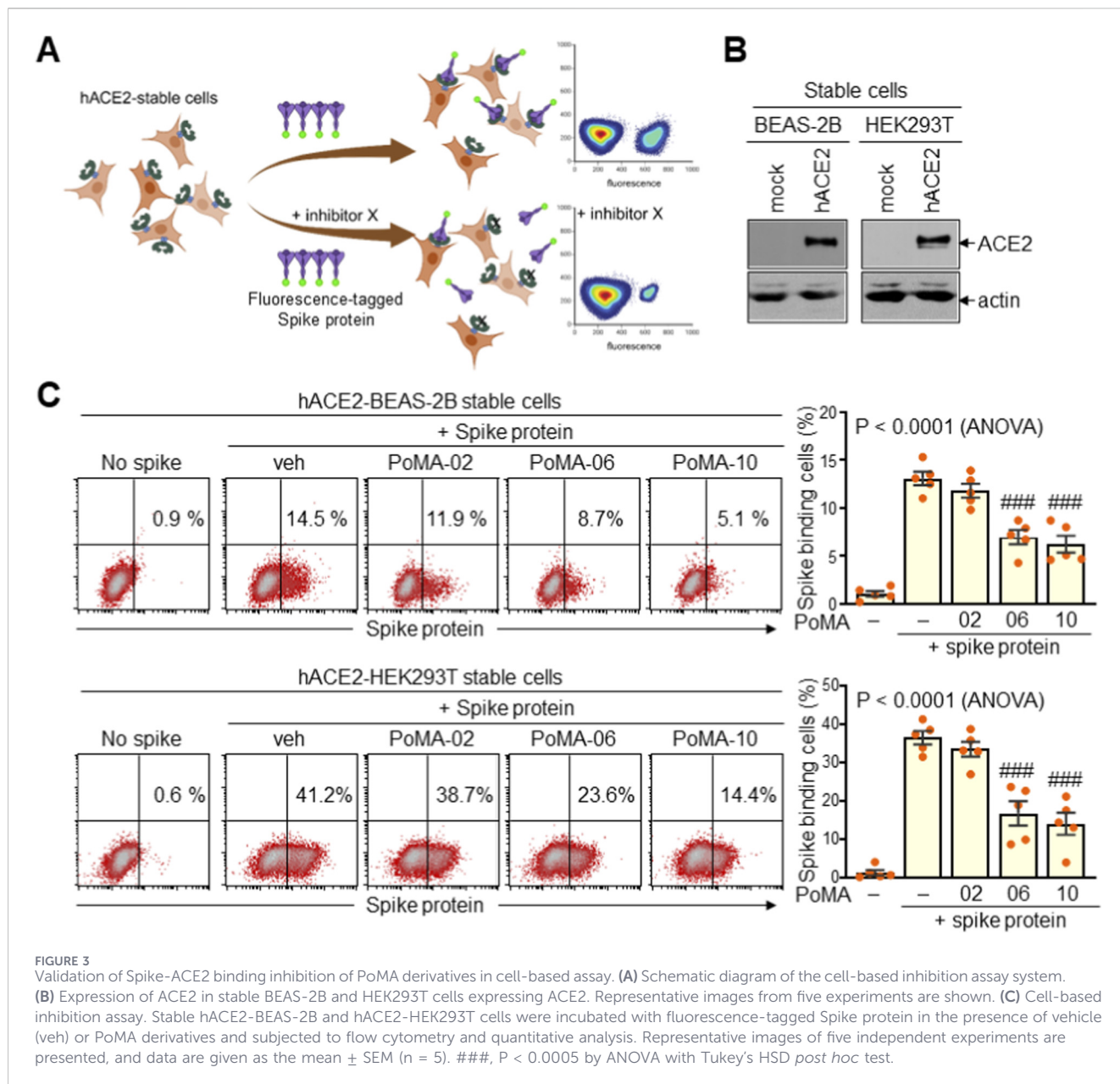
All experiments using SARS-CoV-2 were performed at Institut Pasteur Korea according to the guidelines of the Korea National Institute of Health, as reported previously (Jeon et al., 2020). In brief, Vero cells (American Type Culture Collection, CCL-81) were treated with compounds at concentrations ranging from 0.1 to 100 μ M. Plates were transferred to the BSL3 containment facility and infected with SARS-CoV-2 (ancestral 0.025 MOI; Gamma 0.02 MOI; Delta 0.02 MOI; Omicron 0.045 MOI) for an additional 24 h or 48 h (for Omicron infection). Cells were incubated with anti-SARS-CoV-2 nucleocapsid antibody and Alexa Fluor 488-conjugated secondary antibody, followed by Hoechst 33342 staining. Fluorescent cells were analyzed by Operetta high-content image analysis (Perkin Elmer, Waltham, MA, United States), and the acquired images were analyzed using in-house Columbus software to quantify the cell numbers, infection ratios, and antiviral activity (Wang et al., 2022).

2.10 Pulmonary damage *in vitro* and *in vivo*

BEAS-2B and A549 (ATCC, CCL-185) lung epithelial cells were treated with 50 μ M of amodiaquine (AQ, A2799, Sigma-Aldrich) to induce epithelial cell damage (Lee et al., 2024) and incubated with PoMA-10 (100 μ M) for 24 h. Cells were harvested and subjected to reverse transcription and real-time PCR of human IL-8. For the *in vivo* assay against lung damage, 10-week-old C57BL/6 male mice were injected intraperitoneally for 5 days with DMSO ($n = 6$) or PoMA-10 (20 mg/kg, $n = 6$). Mice were anesthetized by intraperitoneal injection of Avertin and treated with LPS (5 mg/kg) by intratracheal instillation. After 48 h, mice were euthanized by CO₂ inhalation using a gradual fill method (30%–70% displacement/min), followed by the collection of lung and spleen samples. All animal experiments were approved by the IACUC of Ewha Womans University (IACUC-21-072) and conducted in accordance with the international animal welfare guidelines.

2.11 Quantitative real-time PCR (qPCR)

Total RNA was harvested from cells and tissues and subjected to reverse transcription and qPCR using a cDNA synthesis kit and SyBr Green qPCR master mix (Thermo Fisher Scientific). Primer sets for qPCR were used as follows: 5'-aggctcagcttttccaag-3' and 5'-acttctca caaccctctg-3' for human IL-8; 5'-catgtacgttctatcaggc-3' and 5'-ctc ctaatgtcacgcagat-3' for human actin; 5'-accactcacaagtcggagg-3' and 5'-tccaggtagctatggtactcc-3' for mouse IL-6; 5'-tggaccttcaggat gaggac-3' and 5'-ttgtcgttctgttctcc-3' for mouse IL-1 β ; and 5'-aga ggaaatcgtgcgtgac-3' and 5'-tggatgccacaggattcc-3' for mouse actin.



Relative gene expression levels were determined by normalization to actin levels.

2.12 H&E staining of lung tissue

Lung tissues were excised from LPS-administered mice pretreated with vehicle or PoMA-10 and sectioned at 4- μ m thickness. Tissue sections were stained with an H&E staining kit (Abcam, AB245880) and then examined under a light microscope (Nikon Eclipse Ci, Nikon, Japan).

2.13 Statistical analysis

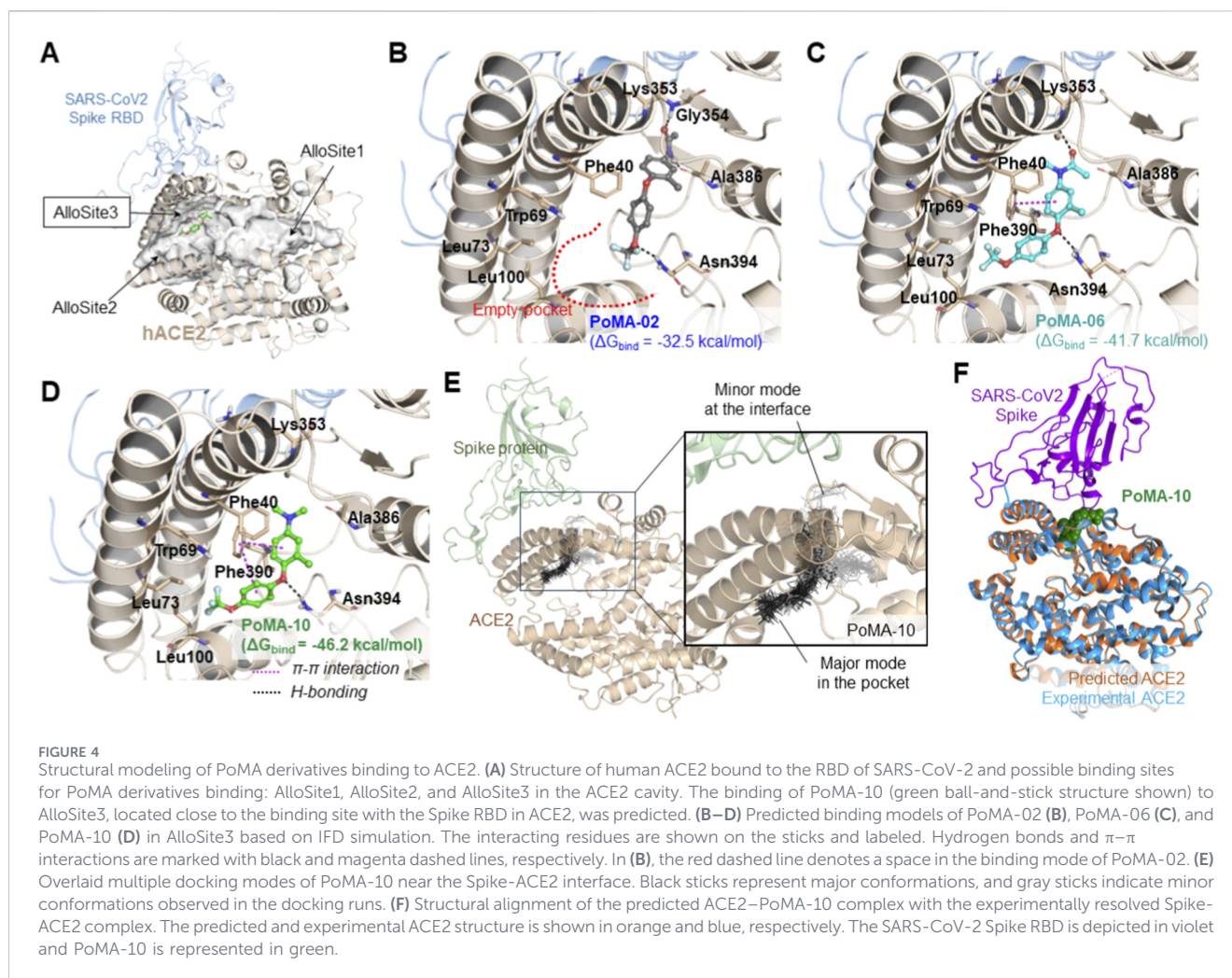
All experiments were performed independently at least five times, and the data are expressed as the mean \pm standard error of the mean (SEM). Statistical significance was determined using a

two-tailed Student's t-test for comparisons between two groups, or one-way analysis of variance (ANOVA) followed by Tukey's HSD *post hoc* test for multiple comparisons. A P value of <0.05 were considered statistically significant.

3 Results

3.1 Identification of Spike-ACE2 binding inhibitors among small molecules

To discover small molecules capable of inhibiting SARS-CoV-2 entry by disturbing the Spike-ACE2 interaction, we performed an inhibition assay using a luminescence-based Spike-ACE2 binding model. Luminescence increases upon Spike-ACE2 binding and decreases when binding is blocked, providing a robust platform



for screening (Figure 1A). We tested antiviral agents (RDS and CQ), membrane receptor inhibitors (CAP, CM, and NM) (Hoffmann et al., 2021; Hoffmann et al., 2020c; Gao et al., 2021), and various diphenyl ether analogs (Figure 1B). As expected, RDS and CQ, which act on viral replication (Hoffmann et al., 2020b), did not interfere directly with Spike-ACE2 binding. CAP, CM, and NM, which target viral proteins, failed to affect the interaction. In contrast, screening of diphenyl ether derivatives (CP1-CP3) and functional peptides (CP4 and CP5) identified CP3 as a potent inhibitor of Spike-ACE2 binding (Figure 1C).

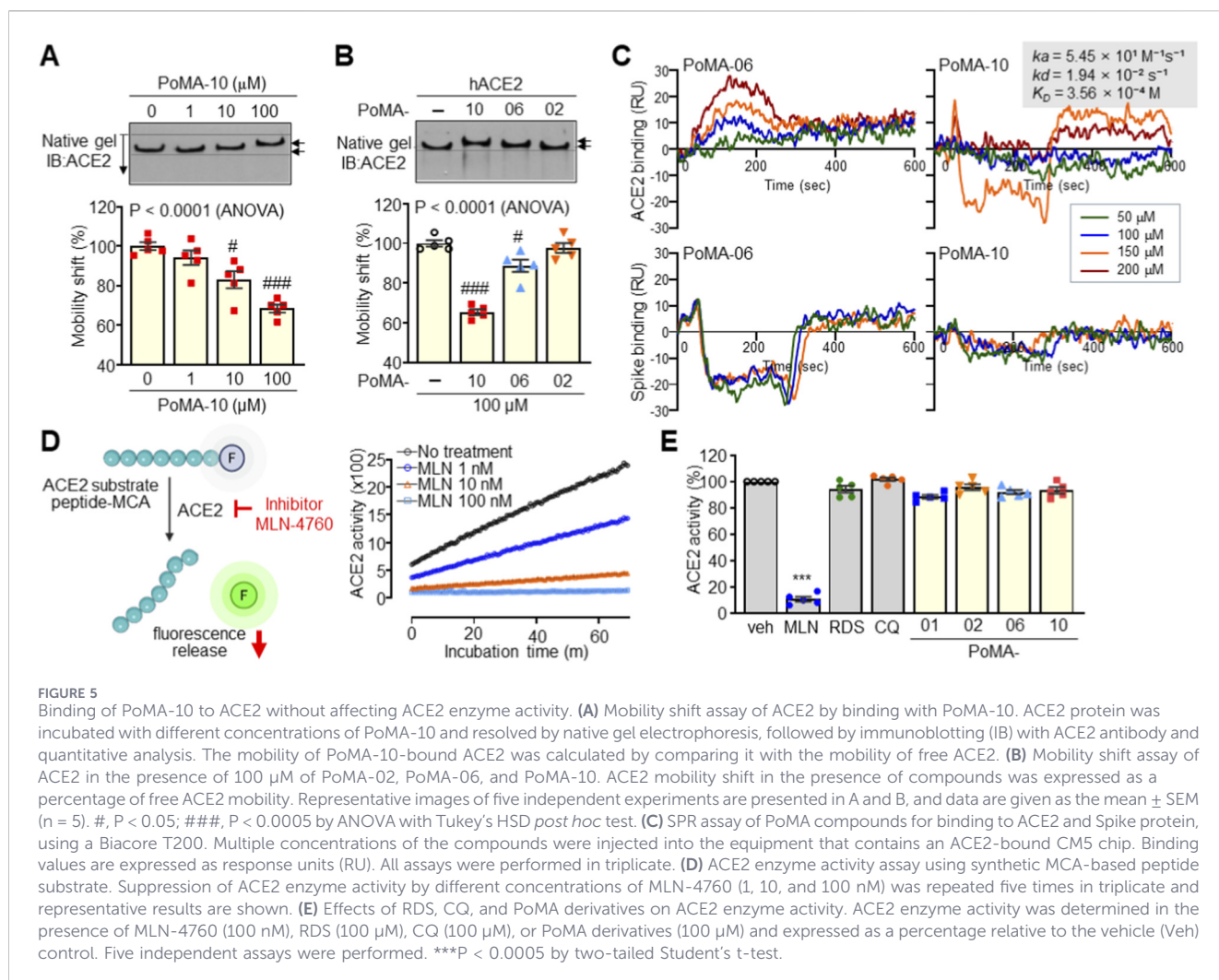
3.2 Structural optimization of PoMA-01 for enhanced Spike-ACE2 binding inhibition

To enhance inhibitory efficacy, we performed rational structural optimization of CP3, hereafter referred to as phenoxy-methylaniline-01 (PoMA-01). Building on the diphenyl ether scaffold, we introduced modifications, including trifluoromethoxy, trifluoromethyl, and fluorine substitutions on the left aromatic ring, and methylation of the amine group on the right aromatic ring (Figure 2A) (Lee et al., 2024). Compounds bearing trifluoromethoxy, trifluoromethyl, or fluorine alone did not significantly inhibit binding. However, PoMA-06, which contains a

trifluoromethoxy group and an *N*-methylacetamide, exhibited enhanced inhibition. Further modification yielded PoMA-10, in which the acetyl group was replaced with a methyl group. PoMA-10 demonstrated superior inhibition of Spike-ACE2 binding (Figure 2B), underscoring the importance of both the trifluoromethoxy and dimethyl substitutions. These findings were confirmed using the ACE2:Spike RBD (SARS-CoV-2) inhibitor screening assay, where PoMA-06 and PoMA-10 both significantly reduced the binding of the Spike RBD to plate-bound ACE2 (Figure 2C).

3.3 Inhibition of spike binding to ACE2-expressing cells

We next evaluated whether PoMA-06 and PoMA-10 could inhibit Spike binding to ACE2 on the cell surface. Stable ACE2-expressing human cell lines were established in normal lung epithelial BEAS-2B and transformed HEK293 via transfection with human ACE2, with high expression confirmed by immunoblotting (Figures 3A,B). Cells were treated with PoMA-02, PoMA-06, and PoMA-10—all containing a trifluoromethoxy group—and binding of fluorescently tagged Spike protein was assessed by flow cytometry. While PoMA-02 showed no effect,



PoMA-06 and PoMA-10 significantly reduced Spike binding to ACE2-expressing cells, with PoMA-10 exhibiting stronger inhibition (Figure 3C). These results confirm that PoMA-10 effectively disrupts Spike protein binding to ACE2 on the cell membrane.

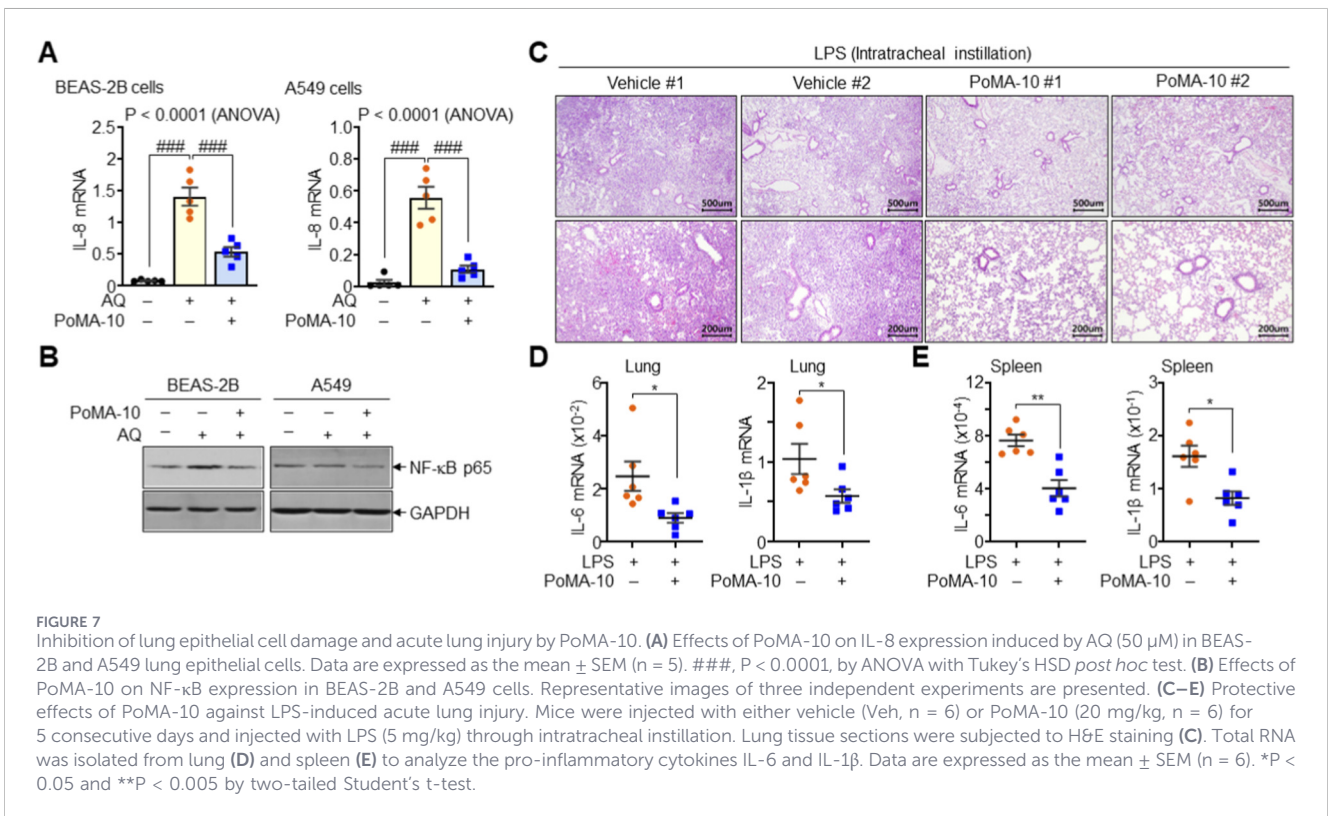
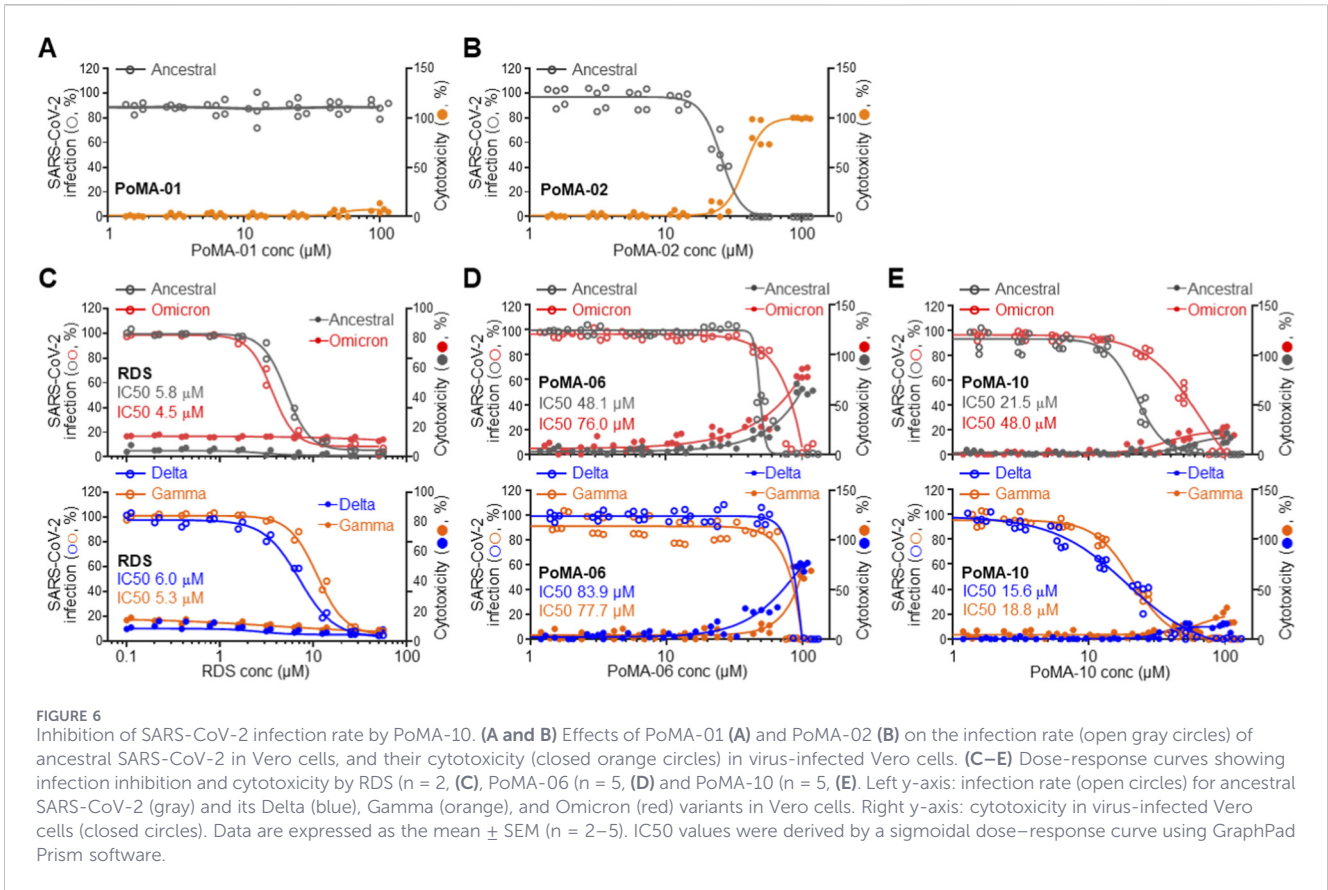
3.4 Predicted binding site of PoMA compounds on ACE2

We then examined whether PoMA derivatives directly interact with ACE2 and modulate the Spike-ACE2 complex. AlloFinder and CAVER analyses (Dutta, 2022) identified three allosteric sites in ACE2, of which AlloSite3—adjacent to the Spike-binding interface—was the most favorable (Baig et al., 2020; Mackin et al., 2022). IFD simulations predicted stable binding of PoMA-06 and PoMA-10 at AlloSite3, whereas PoMA-02 showed unstable interactions and failed to bind persistently (Figure 4A,B; Supplementary Figure S1–S3). PoMA-06 formed stable π - π interactions with F390 and hydrogen bonds with K353 and N394, and PoMA-10 formed additional interactions, including its trifluoromethoxy group with L100 (Figure 4C,D). Prime MM-GBSA rescoring (OPLS4/VSGB) yielded ΔG_{bind} values of -46.2 , -41.7 , and -32.5 kcal^{-1} for PoMA-10, PoMA-06, and PoMA-02,

respectively, supporting PoMA-10 as the strongest binder at AlloSite3. MD simulations confirmed that the ACE2–PoMA-10 complex retained a conformation close to apo ACE2 ($\text{Ca RMSD} < 2 \text{ \AA}$) (Figure 4E,F). Over 300 ns, the Spike protein progressively engaged apo ACE2 with inter-residue distances falling below 3.5 \AA , whereas PoMA-10 increased interfacial fluctuations and reduced residue-level contacts ($< 3.5 \text{ \AA}$) between Spike and ACE2 (Supplementary Videos S1, S2; Supplementary Figure S4–S6). These data indicate that PoMA-10 disrupts stable Spike-ACE2 binding via interface-adjacent modulation, likely through steric or electrostatic effects.

3.5 Direct binding of PoMA-10 to ACE2 without affecting enzymatic activity

We then validated direct binding of PoMA-10 to ACE2 using native polyacrylamide gel electrophoresis. PoMA-10 treatment induced a significant mobility shift of intracellular ACE2 protein at a concentration of 100 μM (Figure 5A). PoMA-02 had no significant effect, whereas PoMA-06 slightly delayed ACE2 protein mobility (Figure 5B). Further SPR analyses demonstrated that PoMA-06 and PoMA-10 exhibited negligible binding affinity for the Spike protein, whereas they showed



distinct interaction profiles with the ACE2 protein (Figure 5C). PoMA-06 displayed a concentration-dependent association with ACE2 but failed to reach a clear saturation point, suggesting a relatively weak or transient binding mode. In contrast, PoMA-10 demonstrated a robust dose-dependent association with ACE2. Kinetic analysis of the PoMA-10/ACE2 interaction revealed an association rate constant (k_a) of $5.45 \times 10 \text{ M}^{-1}\text{s}^{-1}$ and a dissociation rate constant (k_d) of $1.94 \times 10^{-2} \text{ s}^{-1}$. The resulting equilibrium dissociation constant (K_D) was calculated to be $3.56 \times 10^{-4} \text{ M}$ (356 μM). While the binding affinity falls within the high micromolar range—a characteristic frequently observed in low-molecular-weight allosteric modulators—the sensorgrams clearly demonstrate specific, reproducible target engagement. We also confirmed that the known ACE2 inhibitor, MLN-4760, suppressed ACE2 enzymatic activity at the nanomolar concentration. PoMA-10, RDS, and CQ did not affect ACE2 activity, even at a high concentration of 100 μM (Figures 5D,E). These findings demonstrate that PoMA-10 directly binds ACE2 without compromising its enzymatic function.

3.6 Inhibition of SARS-CoV-2 infection in vero cells by PoMA-10

To assess the antiviral activity of PoMA-10 against SARS-CoV-2 infection, we measured the infection rates of the ancestral SARS-CoV-2 and major variants in Vero cells. PoMA-01 had no effect on cell viability or infection, whereas PoMA-02 reduced infection only at cytotoxic concentration (Figure 6A,B). The antiviral RDS, used as a positive control, dose-dependently reduced the infection rates of the ancestral SARS-CoV-2 and major variants, with IC50 values below 10 μM (Figure 6C). PoMA-06 showed weak antiviral activity against the ancestral SARS-CoV-2 and major variants with IC50 values above 50 μM , along with cytotoxicity (Figure 6D). In contrast, PoMA-10 exhibited low cytotoxicity and potent inhibition (IC50 = 21.5 μM) against the ancestral virus, retaining significant activity against Delta and Gamma, and moderate potency against Omicron (Figure 6E). These results suggest the potential of PoMA-10 as an antiviral agent against infectious disease caused by diverse SARS-CoV-2 variants.

3.7 Protective effects of PoMA-10 against lung injury

Given its structural similarity to MPoMA, a known anti-inflammatory compound (Lee et al., 2024), we investigated whether PoMA-10 affects IL-8 expression in BEAS-2B and A549 lung epithelial cells damaged by high concentrations of amodiaquine (AQ). In BEAS-2B and A549 cells, AQ significantly increased IL-8 expression, a response that was markedly reduced by PoMA-10 (Figure 7A). Furthermore, PoMA-10 suppressed the expression of the inflammatory mediator NF- κB (Figure 7B), collectively indicating that PoMA-10 exerts both anti-inflammatory activity and cytoprotective effects on lung epithelial cells. In an LPS-induced mouse model of acute lung injury, intraperitoneal injection of PoMA-10 markedly reduced immune cell infiltration and tissue damage (Figure 7C). Levels of the pro-inflammatory cytokines IL-6 and IL-1 β in the lung and spleen were also significantly decreased by PoMA-10 treatment (Figures 7D,E).

These results definitively show that PoMA-10 has significant potential as a therapeutic agent against both virus-induced and inflammation-induced lung damage.

4 Discussion

In this study, we identified PoMA-10 as a lead small molecule that blocks Spike-ACE2 interaction, while exerting potent anti-inflammatory effects. Structural optimization revealed that incorporating a trifluoromethoxy group and an *N,N*-dimethyl substitution were critical to enhancing viral entry inhibition against SARS-CoV-2 and its major variants.

PoMA-10 is derived from a marine-inspired diphenyl ether scaffold (Camilleri et al., 1988; Bunyapaiboonsri et al., 2007). While our previous study on MPoMA demonstrated cytoprotective effects but limited viral entry inhibition (Lee et al., 2024), the structural transition to a trifluoromethoxy group in PoMA-10 proved essential to bridging this gap, successfully achieving both potent antiviral and anti-inflammatory activities.

To validate the direct engagement of PoMA-10 with the host receptor, we performed SPR analysis, which yielded a calculated K_D of 356 μM . While this affinity is moderate, it aligns with the micromolar IC50 values observed in our functional assays. The efficacy of PoMA-10, despite this moderate affinity, is hallmark of interface-adjacent allosteric inhibitors. In such cases, biological activity arises from inducing specific conformational constraints that disrupt protein–protein interactions (PPI) rather than requiring high-affinity occupancy of a primary binding pocket. By modulating ACE2 accessibility to the Spike protein in this manner, PoMA-10 provides a resilient therapeutic strategy that is less susceptible to viral mutations (Awad et al., 2023).

Although the micromolar potency of PoMA-10 is higher than that of direct-acting antivirals like RDS, its clinical value lies in its high genetic barrier to resistance and dual-action capability. The experimental use of 100 μM *in vitro* was intended to delineate maximal inhibitory potential. Crucially our *in vivo* toxicity data (Supplementary Figure S7)—which showed no adverse effects at doses up to 1,000 mg/kg—suggests a remarkably wide therapeutic window. This safety margin supports the feasibility of localized delivery, such as inhalation or intranasal administration, to achieve effective concentrations at the primary respiratory infection site while minimizing systemic exposure.

To ensure clinical relevance, beyond the innate immune-deficient Vero cell model, we validated PoMA-10 in human-derived immunocompetent lines (BEAS-2B and HEK293T), confirming its efficacy in a context mimicking the human respiratory environment. Molecular modeling suggests that PoMA-10 binds to an interface-adjacent site near the Spike-binding interface without affecting ACE2 enzymatic activity, unlike ACE2 inhibitor MLN-4760 (Berenyiova et al., 2021; Nami et al., 2021; Wang et al., 2024). This allosteric modulation is a key advantage; by inducing subtle conformational shifts at the PPI interface rather than blocking the active site, PoMA-10 prevents viral entry without interfering with the essential physiological functions of ACE2.

Notably, our data suggest that PoMA-10's antiviral and anti-inflammatory activities operate via independent, parallel

mechanisms rather than a single causal chain. While a reduction in viral entry naturally leads to decreased pathogen-induced inflammation, the efficacy of PoMA-10 in the sterile LPS-induced lung injury model—where no viral replication occurs—demonstrates a direct, intrinsic anti-inflammatory capacity. This dual-target profile allows PoMA-10 to block extracellular viral entry via ACE2 modulation while simultaneously—likely through cell permeation—inhibiting intracellular NF- κ B-mediated signaling. This ensures that the inflammatory cascade can be mitigated even if some viral particles bypass the initial entry barrier.

Despite these promising findings, further studies on pharmacokinetics and efficacy in SARS-CoV-2-specific models (e.g., K18-hACE2 mice) remain necessary (Yinda et al., 2021; Zheng et al., 2021). Advanced MD-based network analyses, including dynamic cross-correlation matrix and principal component analysis, are planned to further refine our understanding of PoMA-10's host-modulatory mechanisms. Overall, PoMA-10 exhibits a multifunctional profile as a next-generation host-targeted antiviral with robust dual-action benefits.

5 Conclusion

PoMA-10 was identified as a potent small-molecule inhibitor of SARS-CoV-2 entry. By binding directly to an allosteric site on ACE2, it effectively blocked viral entry across multiple variants without compromising the receptor's enzymatic activity. Beyond its antiviral effect, PoMA-10 mitigated inflammatory lung damage, highlighting its potential as a dual-action therapeutic strategy.

Data availability statement

The original contributions presented in the study are included in the article/[Supplementary Material](#), further inquiries can be directed to the corresponding authors.

Ethics statement

Ethical approval was not required for the studies on humans in accordance with the local legislation and institutional requirements because only commercially available established cell lines were used. The animal study was approved by IACUC at Ewha Womans University. The study was conducted in accordance with the local legislation and institutional requirements.

Author contributions

SoL: Data curation, Formal Analysis, Investigation, Methodology, Writing – original draft. SY: Data curation, Formal Analysis, Investigation, Methodology, Writing – original draft. JL: Data curation, Investigation, Methodology, Writing – original draft. JO: Data curation, Formal Analysis, Methodology, Writing – original draft. J-SR: Investigation, Methodology, Supervision, Writing – review and editing. GK: Investigation,

Methodology, Writing – original draft. HK: Methodology, Software, Visualization, Writing – original draft. NJ: Investigation, Methodology, Software, Visualization, Writing – original draft. SeL: Data curation, Methodology, Software, Supervision, Visualization, Writing – review and editing. SJ: Funding acquisition, Investigation, Methodology, Resources, Writing – review and editing. YL: Methodology, Software, Supervision, Visualization, Writing – review and editing. YP: Funding acquisition, Investigation, Methodology, Project administration, Validation, Writing – review and editing, Writing – original draft. ESH: Conceptualization, Funding acquisition, Investigation, Project administration, Resources, Software, Supervision, Validation, Visualization, Writing – original draft, Writing – review and editing.

Funding

The author(s) declared that financial support was received for this work and/or its publication. This work was supported by the grants of the National Research Foundation (RS-2025-00558072 for ESH; RS-2022-NR074952 for YP; RS-2021-NF000578 for ESH and YP) and Korea Basic Science Institute (National Facilities and Equipment Center) (RS-2024-00401816 for SJ) funded by the Ministry of Science and ICT.

Acknowledgements

We thank Dr. Eun-Yi Moon for providing the human ACE2 expression vector. Schematic illustrations in the figures were generated with the support of Biorender (www.biorender.com).

Conflict of interest

Authors HK and SeL were employed by HITS Inc.

The remaining author(s) declared that this work was conducted in the absence of any commercial or financial relationships that could be construed as a potential conflict of interest.

Generative AI statement

The author(s) declared that generative AI was used in the creation of this manuscript. For language refinement, grammar correction, and overall improvement of readability and clarity throughout the manuscript. Specifically, a large language model (LLM), such as OpenAI GPT-5, was employed for this purpose. The AI-generated text was thoroughly reviewed, edited, and approved by the author(s) to ensure accuracy, scientific integrity, and adherence to the manuscript's content. The primary goal was to enhance the linguistic quality without altering the scientific content or conclusions.

Any alternative text (alt text) provided alongside figures in this article has been generated by Frontiers with the support of artificial intelligence and reasonable efforts have been made to ensure

accuracy, including review by the authors wherever possible. If you identify any issues, please contact us.

Publisher's note

All claims expressed in this article are solely those of the authors and do not necessarily represent those of their affiliated organizations, or those of the publisher, the editors and the reviewers. Any product

that may be evaluated in this article, or claim that may be made by its manufacturer, is not guaranteed or endorsed by the publisher.

Supplementary material

The Supplementary Material for this article can be found online at: <https://www.frontiersin.org/articles/10.3389/fphar.2026.1755268/full#supplementary-material>

References

- Andersen, K. G., Rambaut, A., Lipkin, W. I., Holmes, E. C., and Garry, R. F. (2020). The proximal origin of SARS-CoV-2. *Nat. Med.* 26, 450–452. doi:10.1038/s41591-020-0820-9
- Awad, A. M., Hansen, K., Del Rio, D., Flores, D., Barghash, R. F., Kakkola, L., et al. (2023). Insights into COVID-19: perspectives on drug remedies and host cell responses. *Biomolecules* 13, 1452. doi:10.3390/biom13101452
- Baig, M. S., Alagumuthu, M., Rajpoot, S., and Saqib, U. (2020). Identification of a potential peptide inhibitor of SARS-CoV-2 targeting its entry into the host cells. *Drugs R. D.* 20 (3), 161–169. doi:10.1007/s40268-020-00312-5
- Berenyiova, A., Bernatova, I., Zemancikova, A., Drobna, M., Cebova, M., Golas, S., et al. (2021). Vascular effects of low-dose ACE2 inhibitor MLN-4760-Benefit or detriment in essential hypertension? *Biomedicines* 10, 38. doi:10.3390/biomedicines10010038
- Billah, M. A., Miah, M. M., and Khan, M. N. (2020). Reproductive number of coronavirus: a systematic review and meta-analysis based on global level evidence. *PLoS One* 15, e0242128. doi:10.1371/journal.pone.0242128
- Bunyapiboonsri, T., Yoiprommarat, S., Intereya, K., and Kocharin, K. (2007). New diphenyl ethers from the insect pathogenic fungus *cordyceps* sp. BCC 1861. *Chem. Pharm. Bull. (Tokyo)* 55, 304–307. doi:10.1248/cpb.55.304
- Camilleri, P., Weaver, K., Clark, M. T., Bowyer, J. R., and Hallahan, B. J. (1988). Some novel diphenyl ether herbicides with peroxidizing activity. *J. Agric. Food Chem.* 36, 1061–1063. doi:10.1021/jf00083a037
- Chen, Y., Li, S., Wu, W., Geng, S., and Mao, M. (2022). Distinct mutations and lineages of SARS-CoV-2 virus in the early phase of COVID-19 pandemic and subsequent 1-year global expansion. *J. Med. Virol.* 94, 2035–2049. doi:10.1002/jmv.27580
- Chitsike, L., and Duerksen-Hughes, P. (2021). Keep out! SARS-CoV-2 entry inhibitors: their role and utility as COVID-19 therapeutics. *Virol. J.* 18, 154. doi:10.1186/s12985-021-01624-x
- Cui, W., Duan, Y., Gao, Y., Wang, W., and Yang, H. (2024). Structural review of SARS-CoV-2 antiviral targets. *Structure* 32, 1301–1321. doi:10.1016/j.str.2024.08.005
- Dong, M., Galvan Achi, J. M., Du, R., Rong, L., and Cui, Q. (2024). Development of SARS-CoV-2 entry antivirals. *Cell Insight* 3, 100144. doi:10.1016/j.cellin.2023.100144
- Dutta, K. (2022). Allosteric site of ACE-2 as a drug target for COVID-19. *ACS Pharmacol. Transl. Sci.* 5, 179–182. doi:10.1021/acsp.2c00003
- Gao, W. C., Ma, X., Wang, P., He, X. Y., Zheng, Y. T., Liu, F. L., et al. (2021). Captopril alleviates lung inflammation in SARS-CoV-2-infected hypertensive mice. *Zool. Res.* 42, 633–636. doi:10.24272/j.issn.2095-8137.2021.206
- Haranahalli, K., Honda, T., and Ojima, I. (2019). Recent progress in the strategic incorporation of fluorine into medicinally active compounds. *J. Fluor Chem.* 217, 29–40. doi:10.1016/j.jfluchem.2018.11.002
- Hoffmann, M., Hofmann-Winkler, H., Smith, J. C., Krüger, N., Arora, P., Sørensen, L. K., et al. (2021). Camostat mesylate inhibits SARS-CoV-2 activation by TMPRSS2-related proteases and its metabolite GBPA exerts antiviral activity. *eBioMedicine*. 65, 103255. doi:10.1016/j.ebiom.2021.103255
- Hoffmann, M., Kleine-Weber, H., Schroeder, S., Krüger, N., Herrler, T., Erichsen, S., et al. (2020a). SARS-CoV-2 cell entry depends on ACE2 and TMPRSS2 and is blocked by a clinically proven protease inhibitor. *Cell* 181, 271–280 e278. doi:10.1016/j.cell.2020.02.052
- Hoffmann, M., Mosbauer, K., Hofmann-Winkler, H., Kaul, A., Kleine-Weber, H., Krüger, N., et al. (2020b). Chloroquine does not inhibit infection of human lung cells with SARS-CoV-2. *Nature* 585, 588–590. doi:10.1038/s41586-020-2575-3
- Hoffmann, M., Schroeder, S., Kleine-Weber, H., Müller, M. A., Drosten, C., and Pöhlmann, S. (2020c). Nafamostat mesylate blocks activation of SARS-CoV-2: new treatment option for COVID-19. *Antimicrob. Agents Chemother.* 64. doi:10.1128/AAC.00754-20
- Hu, Y., Lewandowski, E. M., Tan, H., Zhang, X., Morgan, R. T., Zhang, X., et al. (2023). Naturally occurring mutations of SARS-CoV-2 main protease confer drug resistance to nirmatrelvir. *ACS Cent. Sci.* 9, 1658–1669. doi:10.1021/acscentsci.3c00538
- Iketani, S., Mohri, H., Culbertson, B., Hong, S. J., Duan, Y., Luck, M. I., et al. (2023). Multiple pathways for SARS-CoV-2 resistance to nirmatrelvir. *Nature* 613, 558–564. doi:10.1038/s41586-022-05514-2
- Jackson, C. B., Farzan, M., Chen, B., and Choe, H. (2022). Mechanisms of SARS-CoV-2 entry into cells. *Nat. Rev. Mol. Cell Biol.* 23, 3–20. doi:10.1038/s41580-021-00418-x
- Jeon, S., Ko, M., Lee, J., Choi, I., Byun, S. Y., Park, S., et al. (2020). Identification of antiviral drug candidates against SARS-CoV-2 from FDA-approved drugs. *Antimicrob. Agents Chemother.* 64, e00819–e00820. doi:10.1128/AAC.00819-20
- Jochmans, D., Liu, C., Donckers, K., Stoycheva, A., Boland, S., Stevens, S. K., et al. (2023). The substitutions L50F, E166A, and L167F in SARS-CoV-2 3CLpro are selected by a protease inhibitor *in vitro* and confer resistance to nirmatrelvir. *mBio* 14, e0281522. doi:10.1128/mbio.02815-22
- Kiso, M., Yamayoshi, S., Iida, S., Furusawa, Y., Hirata, Y., Uraki, R., et al. (2023). *In vitro* and *in vivo* characterization of SARS-CoV-2 resistance to ensitrelvir. *Nat. Commun.* 14, 4231. doi:10.1038/s41467-023-40018-1
- Kronenberger, T., Laufer, S. A., and Pillaiyar, T. (2023). COVID-19 therapeutics: small-molecule drug development targeting SARS-CoV-2 main protease. *Drug Discov. Today* 28, 103579. doi:10.1016/j.drudis.2023.103579
- Lee, S., Yoon, S. J., Oh, J. H., Ryu, J. S., Park, Y., and Hwang, E. S. (2024). MPoMA protects against lung epithelial cell injury via p65 degradation. *Biomed. Pharmacother.* 175, 116674. doi:10.1016/j.biopha.2024.116674
- Liu, J., Lin, W. K., Sorochinsky, A. E., Butler, G., Landa, A., Han, J. L., et al. (2022). Successful trifluoromethoxy-containing pharmaceuticals and agrochemicals. *J. Fluor. Chem.* 257, 109978. doi:10.1016/j.jfluchem.2022.109978
- Mackin, R. T., Edwards, J. V., Atuk, E. B., Beltrami, N., Condon, B. D., Jayawickramarajah, J., et al. (2022). Structure/function analysis of truncated amino-terminal ACE2 peptide analogs that bind to SARS-CoV-2 spike glycoprotein. *Molecules* 27 (7), 2070. doi:10.3390/molecules27072070
- Meganck, R. M., and Baric, R. S. (2021). Developing therapeutic approaches for twenty-first-century emerging infectious viral diseases. *Nat. Med.* 27, 401–410. doi:10.1038/s41591-021-01282-0
- Moghadas, S. A., Heilmann, E., Khalil, A. M., Nnabuife, C., Kearns, F. L., Ye, C., et al. (2023). Transmissible SARS-CoV-2 variants with resistance to clinical protease inhibitors. *Sci. Adv.* 9, eade8778. doi:10.1126/sciadv.ade8778
- Nair, A. S., Singh, A. K., Kumar, A., Kumar, S., Sukumaran, S., Koyiparambath, V. P., et al. (2022). FDA-approved trifluoromethyl group-containing drugs: a review of 20 years. *Processes* 10, 2054. doi:10.3390/pr10102054
- Nami, B., Ghanaeian, A., Ghanaeian, K., Hour, R., Nami, N., Ghasemi-Dizgah, A., et al. (2021). The interaction of the severe acute respiratory syndrome coronavirus 2 spike protein with drug-inhibited angiotensin converting enzyme 2 studied by molecular dynamics simulation. *J. Hypertens.* 39, 1705–1716. doi:10.1097/HJH.0000000000002829
- Narayanan, S. A., Jamison, D. A., Jr., Guarnieri, J. W., Zaksas, V., Topper, M., Koutnik, A. P., et al. (2024). A comprehensive SARS-CoV-2 and COVID-19 review, part 2: host extracellular to systemic effects of SARS-CoV-2 infection. *Eur. J. Hum. Genet.* 32, 10–20. doi:10.1038/s41431-023-01462-1
- Park, Y., Bae, S. Y., Hah, J. M., Lee, S. K., and Ryu, J. S. (2015). Synthesis of stereochemically diverse cyclic analogs of tubulysins. *Bioorg Med. Chem.* 23, 6827–6843. doi:10.1016/j.bmc.2015.10.003
- Peck, K. M., and Lauring, A. S. (2018). Complexities of viral mutation rates. *J. Virol.* 92. doi:10.1128/JVI.01031-17
- Scovino, A. M., Dahab, E. C., Vieira, G. F., Freire-de-Lima, L., Freire-de-Lima, C. G., and Morrot, A. (2022). SARS-CoV-2's variants of concern: a brief characterization. *Front. Immunol.* 13, 834098. doi:10.3389/fimmu.2022.834098
- Shapira, T., Monreal, I. A., Dion, S. P., Buchholz, D. W., Imbiakha, B., Olmstead, A. D., et al. (2022). A TMPRSS2 inhibitor acts as a pan-SARS-CoV-2 prophylactic and therapeutic. *Nature* 605, 340–348. doi:10.1038/s41586-022-04661-w

- Wang, Q., Zhang, Y., Wu, L., Niu, S., Song, C., Zhang, Z., et al. (2020). Structural and functional basis of SARS-CoV-2 entry by using human ACE2. *Cell* 181, 894–904 e899. doi:10.1016/j.cell.2020.03.045
- Wang, L., Wu, Y., Yao, S., Ge, H., Zhu, Y., Chen, K., et al. (2022). Discovery of potential small molecular SARS-CoV-2 entry blockers targeting the spike protein. *Acta Pharmacol. Sin.* 43, 788–796. doi:10.1038/s41401-021-00735-z
- Wang, J., Beyer, D., Vaccarin, C., He, Y., Tanriver, M., Benoit, R., et al. (2024). Development of radiofluorinated MLN-4760 derivatives for PET imaging of the SARS-CoV-2 entry receptor ACE2. *Eur. J. Nucl. Med. Mol. Imaging* 52, 9–21. doi:10.1007/s00259-024-06831-6
- Yang, L., and Wang, Z. (2023). Bench-to bedside: innovation of small molecule anti-SARS-CoV-2 drugs in China. *Eur. J. Med. Chem.* 257, 115503. doi:10.1016/j.ejmech.2023.115503
- Yinda, C. K., Port, J. R., Bushmaker, T., Offei Owusu, I., Purushotham, J. N., Avanzato, V. A., et al. (2021). K18-hACE2 mice develop respiratory disease resembling severe COVID-19. *PLoS Pathog.* 17 (1), e1009195. doi:10.1371/journal.ppat.1009195
- Zheng, J., Wong, L. R., Li, K., Verma, A. K., Ortiz, M. E., Wohlford-Lenane, C., et al. (2021). COVID-19 treatments and pathogenesis including anosmia in K18-hACE2 mice. *Nature* 589 (7843), 603–607. doi:10.1038/s41586-020-2943-z